The Journal of Chemical Physics ARTICLE pubs.aip.org/aip/jcp

Characterization of diarylethene-based photoswitches with core and valence photoabsorption and photoemission spectroscopies

Cite as: J. Chem. Phys. 164, 124203 (2026); doi: 10.1063/5.0323110
Submitted: 15 January 2026 • Accepted: 11 March 2026 •
Published Online: 30 March 2026

M. Pini,[1] S. Severino,[1] L. Mai,[1] L. Colaizzi,[1] M. Alagia,[2] O. Plekan,[3] R. Richter,[3,a)] E. Arfaoui,[4] F. Montorsi,[4] F. Segatta,[4] M. Garavelli,[4] S. Aloïse,[5] L. Poisson,[6] R. Borrego-Varillas,[7] M. Lucchini,[1,7] M. Coreno,[2,8] M. Nisoli,[1,7] M. Reduzzi,[1,b)] and A. Nenov[4,b)]

AFFILIATIONS

[1] Politecnico di Milano, Physics Department, Piazza Leonardo da Vinci 32, 20133 Milan, Italy
[2] CNR - Istituto Officina dei Materiali (IOM), Laboratorio TASC, Area Science Park Basovizza, Trieste, Italy
[3] Elettra-Sincrotrone Trieste, Strada Statale 14 - km 163,5 in AREA Science Park, 34149 Basovizza, Trieste, Italy
[4] Universitá di Bologna - Alma Mater Studiorum, Dipartimento di Chimica Industriale "Toso Montanari," Via Piero Gobetti 85, 40129 Bologna, Italy
[5] LASIRE - Laboratoire de Spectroscopie pour les Interactions, la Réactivité et l'Environnement, Université de Lille, CNRS, UMR 8516, 59500 Lille, France
[6] Université Paris-Saclay, ISMO, CNRS, Rue André Rivière, 91400 Orsay, France
[7] CNR, Istituto di Fotonica e Nanotecnologie, Piazza Leonardo da Vinci 32, 20133 Milan, Italy
[8] ISM-CNR, Istituto di Struttura della Materia, LD2 Unit, 34149 Trieste, Italy

[a)] Deceased.
[b)] **Authors to whom correspondence should be addressed:** maurizio.reduzzi@polimi.it and artur.nenov@unibo.it

ABSTRACT

We investigate the electronic structure of two dithienylethene (DTE) molecular photoswitches, BTF6 and PTF6, in the gas phase by combining valence photoelectron spectroscopy (PES), x-ray photoelectron spectroscopy, and the near-edge x-ray absorption fine structure. DTEs have attracted significant attention due to their high photoisomerization quantum yield, fatigue resistance, and thermal irreversibility, which underpin applications ranging from molecular machines to photoswitchable biomolecules. Supported by first-principles simulations, our analysis elucidates how the different extent of π-conjugation, arising from the distinct thiophene/benzothiophene subunits, manifests across the various spectroscopic observables. By comparing the calculated signatures of the open- and closed-ring isomers, we further assess the sensitivity of each probe to the structural changes associated with photoinduced cyclization. Overall, these results deliver a detailed picture of the intrinsic electronic properties of DTEs in the gas phase and provide a robust basis for future time-resolved studies of their ultrafast photoisomerization dynamics.

INTRODUCTION

Diarylethenes (DAEs) are a well-known class of photochromic molecules that display a reversible color change upon UV or visible irradiation. Beyond the change in color, these molecules have been used as molecular photoswitches for a variety of technological applications.[1] Dithienylethenes (DTEs) exhibit robust thermal bistability and excellent photoreversibility thanks to linking thiophene rings (and derivatives thereof) to the cyclohexadiene-like reactive core. Upon irradiation, DTEs undergo reversible transformation between two stable isomers, an open-ring (OR) and a closed-ring (CR) one, with different chemical and physical properties (see Fig. 1). This light-induced structural modification consists of a reversible hexatriene (HT) ↔ cyclohexadiene (CHD) electrocyclic reaction of the molecular central unit (highlighted in Fig. 1). Besides their bistability, the significant spectral separation between the absorption spectra of the OR and CR isomers, together with the ultrafast photoswitching processes with good quantum yields and the high fatigue resistance, the combination of photochemical reversibility with thermal irreversibility, and the high photoisomerization quantum yield, make DTEs highly promising candidates for control of molecular functionality, opening a broad range of applications, including molecular electronics, optoelectronic devices, molecular machines, actuators, and data storage systems.[2,3] In addition to that, they can also be used to light-control biological activity when incorporated in biomolecules, leading to photoswitchable DNA,[4] or biological markers.[5]

The electronic structure and photoinduced dynamics of DTEs have been studied in the past, mostly in solution[6,7] or in solid state,[8,9] with theoretical support at various levels of sophistication ranging from semiempirical to multi-reference.[10–21] A notable exception is a recent study of the ultrafast gas phase dynamics by Lietard *et al.*[22] The open-ring DTEs exist in two stable conformations in solution and in gas-phase, parallel [OR(p)] and anti-parallel [OR(ap)], regarding the relative orientation of the thiophene rings (see Fig. 1), characterized by highly non-planar geometrical structures with a strongly disrupted π-system (see Figs. S2 and S3 in the supplementary material for 3D structures). Only the OR(ap) conformer can engage in photocyclization, while the OR(p) conformer is inert. The formation of a single bond between two carbon atoms of the thiophene rings in the course of the electrocyclic reaction leads to a near planarization of the molecule, restoring the delocalization of the π-system over the entire aromatic scaffold explaining why the CR is absorbing in the visible region.

Vacuum ultraviolet (VUV) and x-ray irradiation offer powerful and complementary spectral windows for studying the electronic structure and photoreactivity in the gas phase. Unlike UV/Vis spectroscopy, which detects only optically allowed transitions, VUV and x-ray spectroscopies generate signals from all electronic states because absorption in these energetic regimes is universal. This universality, together with the complementary sensitivity of VUV excitation to delocalized valence orbitals and x-ray excitation to localized core levels, provides detailed information about the intrinsic electronic properties of molecules. In this work, we investigate the gas phase OR conformers of two DTEs, namely 1,2-bis (2-methylbenzo[b] thiophen-3-yl)perfluorocyclopentene (BTF6) ($C_{23}H_{14}F_6S_2$) and 1,2-bis(2,4-dimethyl-5-phenyl-3-thienyl)perfluorocyclopentene (PTF6) ($C_{29}H_{22}F_6S_2$) (see Fig. 1), by means of valence VUV photoelectron spectroscopy (PES), x-ray photoelectron spectroscopy (XPS), and the near-edge x-ray absorption fine structure (NEXAFS) at the sulfur $L_{2,3}$-edge and at the carbon K-edge. The interpretation of the spectra is facilitated by *ab initio* calculations at the level of second-order multi-reference perturbation correction on top of restricted active space self-consistent field theory (i.e., RASSCF/RASPT2).[23–27] The combined experimental and theoretical valence- and core-level spectroscopic characterizations elucidate the different degrees of sensitivity of the aforementioned spectroscopies to the extension of the π-conjugated framework and to its rearrangement in the course of the electrocyclic reaction, as well as to fine structural differences between the two DTE derivatives. Beyond establishing the feasibility of gas phase measurements on these comparatively large DTEs, the present work demonstrates that DTEs are good candidates for future time-resolved studies of photoisomerization dynamics in isolated systems.

This paper is organized as follows: First, we present the experimental and computational methodologies. Then, we compare and analyze the spectral features of recorded and simulated XPS and NEXAFS spectra at the sulfur $L_{2,3}$-edge and at the carbon K-edge, as well as PES spectra for both BTF6 and PTF6 in their parallel and anti-parallel conformations. Finally, owing to the good agreement between theory and experiment, on the example of BTF6, we make predictions regarding the time-resolved XPS, NEXAFS, and PES signatures of the photoinduced electrocyclic reaction.

EXPERIMENTAL METHODS

The measurements on the BTF6 and PTF6 molecular systems presented in the following sections were carried out at the Gas Phase Photoemission (GAPH) beamline of the Elettra Synchrotron in Trieste.[28,29] All photoelectron spectra were recorded using a VG-220i hemispherical analyzer mounted at the magic angle (54.7°) with respect to the linearly polarized incident light beam. In this configuration, the XPS spectra at the S $L_{2,3}$-edge and at the C K-edge have been acquired with a resolution of 200 meV, while the resolution for valence photoelectron spectra is 100 meV. Photoabsorption spectra were acquired by measuring the total ion yield. For the PTF6 molecule, a channel electron multiplier placed near the ionization region was used, whereas for the BTF6 sample, a microchannel plate (MCP) detector coupled to a non-commercial Wiley-McLaren-type time-of-flight mass analyzer was employed. The resolution in the NEXAFS measurements is 30 meV at the S $L_{2,3}$-edge and 50 meV at the C K-edge.

The energy scales for the C K-edge and S $L_{2,3}$-edge spectra were calibrated by simultaneously recording the spectra of the samples and reference gases, CO_2 and SF_6, respectively. XPS spectra of BTF6 and PTF6 at the S 2*p* edge were acquired using a photon energy of 240 eV and calibrated with respect to the S(2p) core-level binding energy (BE) of SF_6 gas (180.2 eV).[30] The XPS spectra at the carbon K-edge for both molecules were recorded with a photon energy of 382 eV and calibrated using the C 1s BE of CO_2 gas (297.7 eV).[31] The SF_6 absorption peaks at 173.44 eV [S $2p_{1/2} \rightarrow a_{1g}$] and 184.57 eV [S $2p_{1/2} \rightarrow t_{2g}$][32] were used to calibrate the S 2p NEXAFS spectra, while the C K-edge NEXAFS spectra were calibrated using the C 1s → π^* at 290.77 eV.[33] PES spectra for both

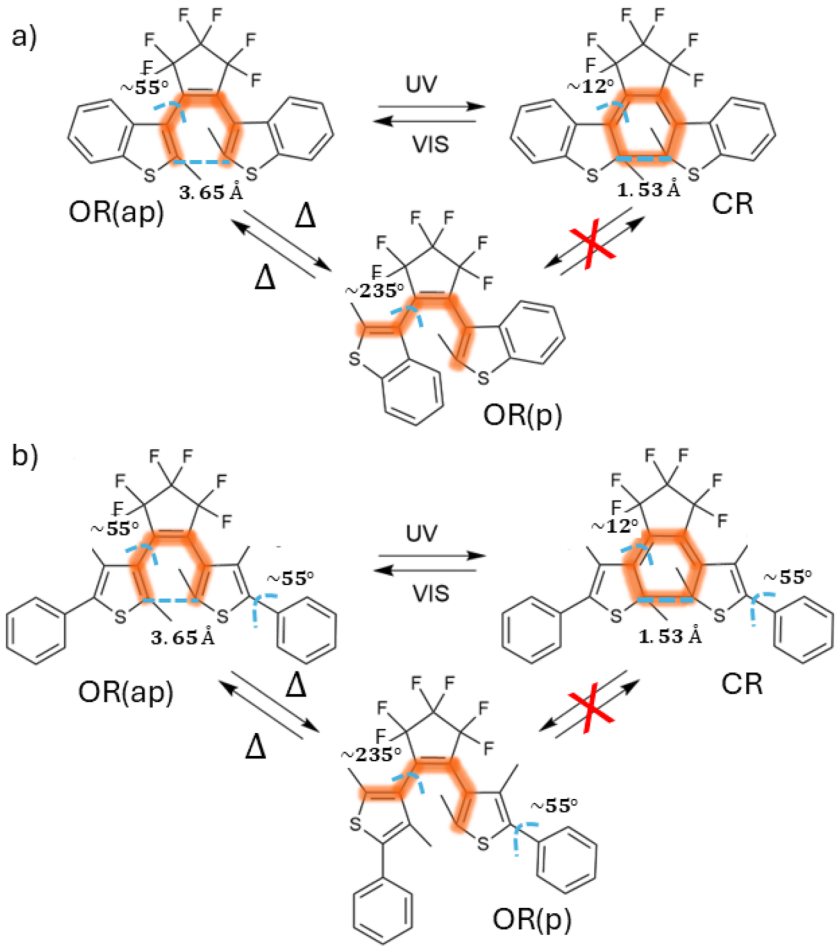

FIG. 1. Chemical structure of the target molecules of this study: (a) BTF6 and (b) PTF6 in their open-ring anti-parallel [OR(ap)], open-ring parallel [OR(p)], and closed-ring (CR) forms, highlighting hexatriene/cyclohexadiene units involved in the electrocyclic reaction, as well as the values of several representative degrees of freedom. Transformation between OR(ap) and OR(p) is facilitated thermally; instead, transformation between OR(ap) and CR is facilitated with UV/Vis light. 3D structures are provided in Fig. S2 of the supplementary material.

molecular samples were acquired using a photon energy of 98.5 eV over a BE range from 6 to 18 eV. The BE scale of the PES spectra for both BTF6 and PTF6 was calibrated using the Ar 3p ($3p_{3/2}$, $3p_{1/2}$) valence spectrum.[34]

The molecular compounds studied here were purchased from TCI Chemicals Europe, with stated purities of 97% for BTF6 and 98% for PTF6. Sublimation into the gas phase within the experimental chamber was achieved by heating the powdered samples to ~65 °C for both molecules. The samples were heated in a crucible terminating in a needle, allowing the sublimated molecules to be directly injected into the interaction chamber. This temperature is well below the melting points of BTF6 (160 °C) and PTF6 (132 °C). During the experiments, the molecular flux and sample purity were continuously monitored by PES and/or mass spectrometry (see the supplementary material), enabling control of the sublimation process as a function of temperature. Raw spectra and background-subtracted spectra are provided in a dedicated repository accessible via the following link: https://doi.org/10.6092/unibo/amsacta/8639.

COMPUTATIONAL DETAILS

The computational protocols for simulating the PES, XPS, and NEXAFS spectra have been presented and thoroughly benchmarked in the past.[25–27,35] In the following, we briefly outline the general structure of the protocol.

The electronic structure calculations were performed at the multi-reference wave function level of theory. Precisely, the wave functions of the electronic ground state and of the valence-ionized, core-ionized, and core-excited states were computed at the state-average (SA)-RASSCF level,[36] whereas the energies were perturbatively corrected at the single state (SS)-RASPT2 level.[36,37] Dyson norms[38] and transition dipole moments between the ground state and the excited states were calculated with the RAS state interaction routine (RASSI) approach using the RASSCF wavefunctions.[39] The RASSI approach was also used to compute spin–orbit coupling (SOC) terms, necessary to reproduce the relativistic effect at the sulfur $L_{2,3}$-edge.

The composition of the active space (AS), i.e., the list of relevant orbitals and electrons for the process under scrutiny, lies at the heart of the RASSCF method. It needs to be suitably adapted to target the electronic states of interest. RASSCF represents a generalization of the complete active space (CAS)SCF method, dividing the AS into three sub-spaces—RAS1, RAS2, and RAS3. This partitioning provides higher flexibility while reducing the computational effort. In the following, we will use the common notation RAS(n,l,m;a,b,c), where the first three labels indicate the number of electrons in the active space, the maximum number of holes in RAS1, and the maximum number of excitations in RAS3, while the last three labels denote the number of orbitals in the three sub-spaces. The strategies for computing valence-ionized (PES), core-ionized (XPS), and core-excited (NEXAFS) states are provided in the supplementary material.

All electronic structure calculations were performed with the software OpenMolcas[40] starting from geometries optimized at the MP2 level with the 6-31G(p) basis set with Gaussian 16, rev. A.03.[41] The atomic natural orbital basis set ANO-R[42] was used throughout with the following contraction scheme: triple-ζ with multiple sets of polarization functions of d- and f-types (the so-called ANO-R2 contraction) for the atom being excited/ionized (specifically, 5s4p3d1f for sulfur and 4s4p2d1f for carbon) and double-ζ with a single set of polarization functions for the remaining atoms (the so-called ANO-R1 contraction). This strategy has been shown to give very similar results to calculations with the ANO-R2 basis set on all "heavy" atoms.[27] Scalar relativistic effects are taken into account via the exact two-component (X2C) Hamiltonian.[43] Perturbation correction to the RASSCF energetics is carried out with an imaginary shift of 0.2 a.u. and Ionization Potential Electron Affinity (IPEA) set to 0.0 a.u., setting the number of frozen orbitals to zero. A density-fitting approximation, known as the Cholesky decomposition[44] of the electron repulsion integrals, was used to speed up the calculation of two-electron integrals. Sub-eV rigid shifts were applied to the spectra to maximize the overlap with the experimental spectra (values provided in the captions of the corresponding figures).

The PES, XPS, and NEXAFS spectra have been computed with the sum-over-states approach, where each BE (PES and XPS) or transition (NEXAFS), computed with respect to the electronic ground state, is convoluted with a Gaussian function weighted by the appropriate Dyson norm (PES and XPS) or the squared module of the transition dipole moment (NEXAFS). The extent of the Gaussian-shaped phenomenological broadening of each individual transition is set by the Gaussian standard deviation σ assigned to the same value for all transitions of a given atom type and adjusted to match the overall experiment bandwidth (values provided in the captions of the corresponding figures).

The OR form exists in two conformations, anti-parallel and parallel. Gas-phase structure optimization in the ground electronic state reveals that the anti-parallel (i.e., reactive) conformers are of *near* C_2 symmetry. The symmetry breaks due to the slight non-planarity of the cyclopentene ring and small variations in the torsional angle of the aromatic residues (benzothiophene in BTF6 and phenylthiophene in PTF6) with respect to the cyclopentene of $\pm 5^\circ$ from the mean value 55°. At variance, the parallel conformers are of C_1 symmetry. Structurally, they differ from the anti-parallel ones merely in the value of one of the two torsional angles, being flipped by 180° (see Fig. S3 of the supplementary material for structural comparison). This has important implications for the spectroscopies simulated in this study. Whereas the stacking pattern changes between parallel and anti-parallel conformations, the extent and strength of the π-interactions remain similar. As a consequence, in the liquid phase, the OR(ap) and OR(p) forms are virtually isoenergetic, meaning that the OR form exists in a mixture of the two conformers with a ratio close to 2:1 for BTF6 and 1:1 for PTF6.[45,46] Consequently, in principle, both conformers need to be considered in the simulation. As shall be demonstrated, VUV photoemission spectroscopy, which directly probes the structure of the frontier orbitals, is indeed sensitive to variations in the stacking pattern as they translate into variations of the energies of the π orbitals (and thus of the associated BEs). X-ray spectroscopies, instead, are to a great extent insensitive to the stacking pattern. Thus, as long as both conformers exhibit comparable π-conjugation (confirmed by the similar torsional angle values), chemical shifts of merely few tens of meV are observed. We demonstrate this on the example of NEXAFS spectra at the carbon K-edge and at the sulfur $L_{2,3}$-edge. In the case of the carbon K-edge, we simulated the NEXAFS signals of the C_1 symmetry OR(p) conformers of BTF6 and PTF6 by explicitly computing the $1s \rightarrow$ LUMO contribution from all (formally nonequivalent) sites (23 carbons in BTF6 and 29 carbons in PTF6) and showed that it is identical to the signals of the C_2 symmetry OR(ap) conformers (see Fig. S10 of the supplementary material). Moreover, we compared the total signal to the one obtained by considering only sites with a unique local coordination environment (12 carbons in BTF6 and 15 carbons in PTF6, Fig. 4). We show that despite the lack of global symmetry, the left and right sides of the OR(p) conformer exhibit nearly identical signals (see Fig. S10 of the supplementary material). These results confirm that x-ray signals are far more sensitive to through-bond (e.g., electronegativity differences and π-conjugation) interactions than to through-space (i.e., dispersion) interactions. This is further confirmed at the sulfur $L_{2,3}$-edge, where the NEXAFS signals of the OR(p) and OR(ap) conformers again coincide (see Fig. S5 of the supplementary material).

The comparison carried out for the OR(p) and OR(ap) conformers justifies the approximation adopted in the rest of this work, namely, to consider only locally unique sites of only the OR(ap) conformer for the simulation of the XPS and NEXAFS spectra. A mixture of OR(ap) and OR(p) was considered in the simulation of the PES signals, with ratios of 2:1 and 1:1 for BTF6 and PTF6, respectively. All input and output files of the calculations are provided in a dedicated repository accessible via the following link: https://doi.org/10.6092/unibo/amsacta/8639.

RESULTS AND DISCUSSION

Sulfur $L_{2,3}$-edge

XPS core-ionization spectra

Figures 2(a) and 2(c) show the experimental and theoretical XPS spectra at the sulfur $L_{2,3}$-edge of BTF6 and PTF6, respectively. The calculated BEs and Dyson norms for the OR(ap) conformer of both molecules are reported in Table I. Both spectra present a double peak feature, common for the XPS spectra of sulfur-containing aromatic compounds,[27,47] arising due to spin–orbit splitting. The agreement between theory and experiment is excellent, with the calculations slightly underestimating (by 0.05 eV) the splitting strength.

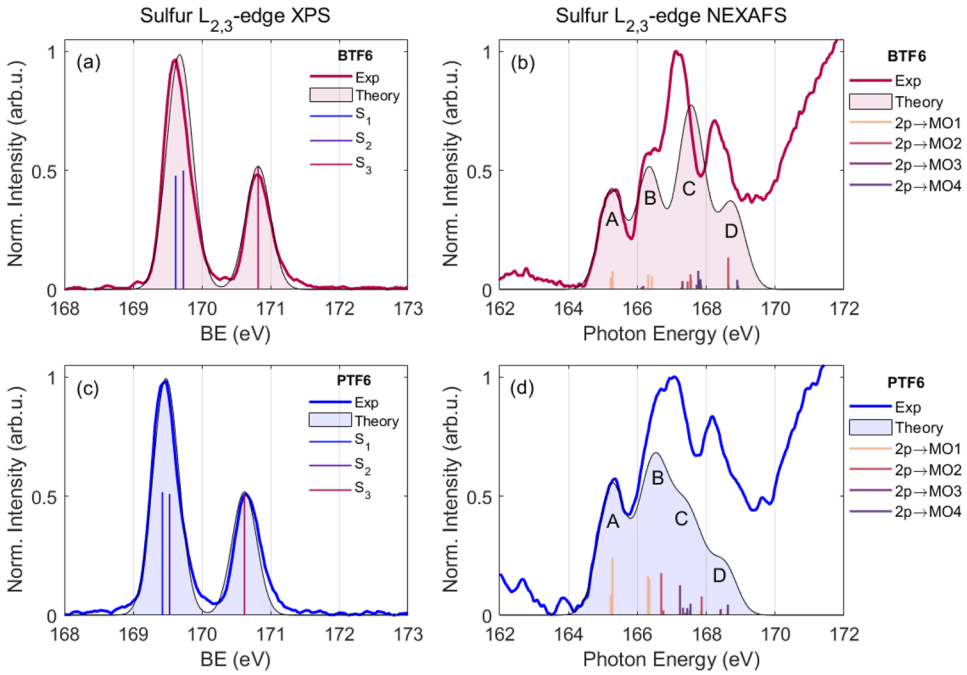

FIG. 2. Experimental data (solid line) and calculated OR(ap) conformer (shaded area) XPS spectra and NEXAFS spectra at the sulfur $L_{2,3}$-edge of (a) and (c) BTF6 and (b) and (d) PTF6 molecules, respectively. The sulfur 2p XPS calculated spectra have been shifted by 0.05 eV for both molecules to match the experimental ones. The calculated NEXAFS spectra have been normalized to the first experimental peak.

TABLE I. Theoretically calculated sulfur $L_{2,3}$-edge binding energies (BEs) of BTF6 and PTF6, with the inclusion of spin–orbit coupling. The reported BE values have been shifted by +0.05 eV for both the molecules as reported in Fig. 2 to match the experimental data. The Dyson norm for all the ionization processes in the two molecules is equal to 1.50.

XPS calculations—sulfur $L_{2,3}$-edge			
	BE (eV)		
	BTF6	PTF6	Leading transition
S_1	169.58	169.43	
S_2	169.68	169.53	S 2p ionization
S_3	170.77	170.62	

The feature at a lower BE is associated with the $2p_{3/2}$ (L_3) state, which possesses a fourfold degeneracy, while the peak at a higher BE corresponds to the twofold degenerate $2p_{1/2}$ (L_2) state.[48] The anisotropy of the molecular field manifests in the further weak splitting of the peak associated with the L_3 state into two components (highlighted as S_1 and S_2 in the two panels of Fig. 2). With the values of 110 and 100 meV for BTF6 and PTF6, respectively, the calculated molecular-field splitting is an order of magnitude smaller compared to the spin–orbit coupling and hardly discernible in the experimental spectra.

The BTF6 spectrum shows a very good agreement with that of bare benzothiophene reported by Toffoli *et al.*[47] The nearly perfect resemblance is rationalized by the localization of the valence molecular orbitals on the benzothiophene fragment in the OR conformer due to the pronounced twist of 55° with respect to the cyclopentene fragment, which reduces the conjugation between them.

The PTF6 spectrum exhibits a redshift of 160 meV with respect to BTF6. In comparison, the XPS spectrum of bare thiophene is blueshifted with respect to benzothiophene,[47] an observation explained by the reduced dimension of the aromatic system. The redshift recorded for PTF6 supports the notion of partial conjugation between the thiophene and the phenyl fragment attached to it. As predicted by the computations, despite the pronounced twist of 55°, the two units are not fully uncoupled. As a further confirmation of the extension of the conjugation, the calculations of 1,2-bis(2,4-dimethyl-3-thienyl)perfluorocyclopentene (TF6), essentially PTF6 stripped of the two phenyl units, report a 200 meV blueshift of the sulfur peak (see Fig. S4 of the supplementary material), placing it above the BE of BTF6 (and similar to the BE of bare thiophene), contrary to what is observed in the experiments. This indicates that extending the conjugated system through the functionalization of thiophene with a phenyl group allows for a better shielding of core-holes compared to functionalization through ring fusion, presumably due to the bigger conjugated system (five double bonds in phenylthiophene compared to four double bonds in benzothiophene).

NEXAFS spectra

The experimental and theoretical NEXAFS spectra at the sulfur $L_{2,3}$-edge for BTF6 and PTF6 are shown in Fig. 2. The corresponding transition energies of the OR(ap) conformer, obtained using both spin-adiabatic and spin-diabatic (singlet and triplet) states, are shown in Fig. 3, along with the associated oscillator strengths. The simulated spectra have been normalized to the first experimental peak at 165 eV instead of the most intense one, the rationale being that the contribution from transitions not considered in the calculations (e.g., transitions to Rydberg- and σ^*-type orbitals, not included

a.

Peak	Energy (eV)	Osc. strength	Leading conf.
A	165.23 - 165.28	0.012	S 2p→MO1
B	166.30 - 166.42	0.009	S 2p→MO1
	166.12 - 166.17	0.002	S 2p→MO3
C	167.46 - 167.55	0.012	S 2p→MO2
	167.27 - 167.31	0.004	S 2p→MO3
	167.72 - 167.83	0.004	S 2p→MO4
	167.82 - 167.85	0.003	S 2p→MO2
D	168.64 - 168.65	0.006	S 2p→MO2
	168.89 - 168.91	0.004	S 2p→MO4
	168.93 - 168.93	0.002	S 2p→MO2

b.

Peak	Energy (eV)	Osc. strength	Leading conf.
A	165.23 - 165.27	0.014	S 2p→MO1
B	166.31 - 166.34	0.011	S 2p→MO1
	166.69 - 166.75	0.009	S 2p→MO2
C	167.24 - 167.32	0.005	S 2p→MO3
	167.40 - 167.54	0.005	S 2p→MO4
	167.86 - 167.87	0.004	S 2p→MO2
D	168.41 - 168.42	0.003	S 2p→MO3
	168.61 - 168.63	0.004	S 2p→MO4

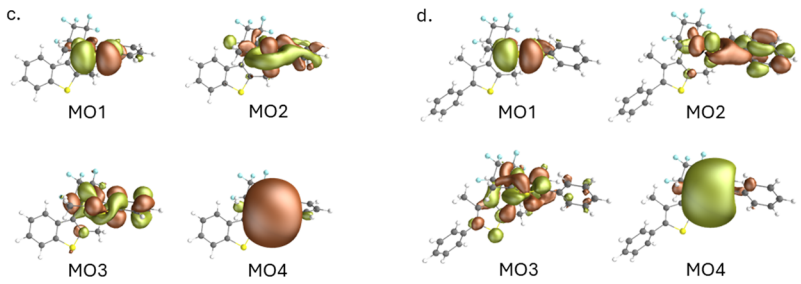

FIG. 3. Theoretically calculated core excited states at the sulfur $L_{2,3}$-edge together with the virtual orbital involved: [(a) and (c)] BTF6 and [(b) and (d)] PTF6. For each peak appearing in the NEXAFS signal, the transition energies and the oscillator strengths are reported in the table.

in the active space) increases with increasing energy. Simulations of benzothiophene at the DFT level, unaffected by active space limitations, clearly demonstrate how the overall NEXAFS spectrum is the aggregation of a vast number of low intensity transitions.[47] Here, we focus on the main contributions to the spectra of BTF6 and PTF6 and refer to the work of Toffoli *et al.* for a detailed analysis.

The experimental NEXAFS spectra are characterized by a three-peak profile in the photon energy range between 164 and 169 eV, common for sulfur-containing organic molecules,[27,47,49,50] with the central peak being considerably broader in PTF6, while showing a shoulder toward lower photon energies in BTF6.

This shape can be explained by accounting for core-transitions toward virtual molecular orbitals of 3d/4s character with a high molecular orbital coefficient on the sulfur (depicted in Fig. 3) and considering spin–orbit splitting. In detail, orbitals MO1 and MO4 are to a large extent uncoupled from the π-system in both molecules. As such, the transition from the 2p orbitals of the sulfur toward these two orbitals is insensitive to its chemical environment, giving rise to transitions at the same energies for both systems. In particular, transitions toward MO1 give rise to signals in the energy range of 165.0–166.3 eV (labeled A in the spectrum), while transitions toward MO4 are responsible for features between 167.5 and 169.0 eV (labeled C and D). In contrast, orbitals MO2 and MO3 show a degree of mixing with the π-system of benzothiophene (BTF6) and phenylthiophene (PTF6), which alter their energies. In particular, in BTF6, the d-orbital on the sulfur interacts only weakly with the benzothiophene π-system for symmetry reasons, while it mixes strongly with the phenyl π-system in PTF6 due to the pronounced twisting of the latter with respect to the thiophene. This leads to a redshift of the MO2 energy in PTF6 and, consequently, to about a 1 eV redshift of the associate core-transition from the energy range of 167.5–169.0 eV in BTF6 to 166.7–168.0 eV in PTF6. Hence, in BTF6, the high energy component of the core-transition to MO1 (166.35 eV, labeled B) and the low energy component of the core-transition to MO2 (167.5 eV, labeled C) appear as distinct peaks, whereas in PTF6, they overlap around 166.5 eV, causing the broadening of the central peak observed experimentally. We note that the calculations overestimate the splitting of peaks B and C.

Similar reasoning can be used to rationalize a redshift of ~1 eV of the core-transition to MO3 in BTF6 with respect to PTF6. For symmetry reasons, the d-orbital on the sulfur couples to the π-system of benzothiophene. Since the transitions to MO3 have low oscillator strengths, the effect on the spectrum is marginal.

Carbon K-edge

XPS core-ionization spectra

The experimental XPS spectra at the carbon K-edge are reported only for BTF6 [Fig. 4(c)] due to problems with the PTF6 sample during data acquisition. The calculated spectra are reported for both systems [Figs. 4(c) and 4(d)]; BE and Dyson norms are reported in Table II. The simulated spectrum is the result of convoluting the contribution of 12 (BTF6)/15 (PTF6) unique carbon atoms (see labeling and color-coding in Fig. 4). In the experimental BTF6 spectrum, the peak at 297.8 eV arises from the CO_2 gas used for calibration purposes. The C 1s XPS spectra of both systems consist of two features, an intense broad peak in the BE range 289.5–292 eV and a less intense sharper one centered at 296 eV. As evidenced by the calculations, the two features derive from carbons experiencing markedly different chemical environments. In fact, the peak at 296 eV arises due to the ionization of carbons C_1 and C_2, and the ~5 eV blueshift with respect to the main spectral feature is due to the immediate vicinity of the strongly electronegative fluorine atoms. The intense peak is the result of contributions from all the remaining carbon atoms. In BTF6, the thiophene carbons of the benzothiophene unit (C_4–C_7) and the two methyl carbons contribute in a BE range of ~600 meV in the higher energy part of the main peak, around 290.8 eV. Instead, the contributions from the benzene carbons of the benzothiophene unit (C_8–C_{11}) are confined in a narrow BE range of ~300 meV in the lower energy part, around 290.2 eV. The main peak of BTF6 shows a shoulder at a higher BE, which is not reproduced by the simulations. The absence of this feature in the calculated spectrum may arise either from vibrational broadening effects that are not explicitly included in the simulation, or from an underestimation of the BE associated with the C_3 carbon, which shifts its contribution to lower energies in the theoretical spectrum. The main peak appears narrower in the simulations of PTF6, as contributions from the thiophene unit (C_4–C_7) appear 0.3 eV redshifted with respect to BTF6 and fall within the same BE window as the contributions from the phenyl carbons (C_8–C_{13}),

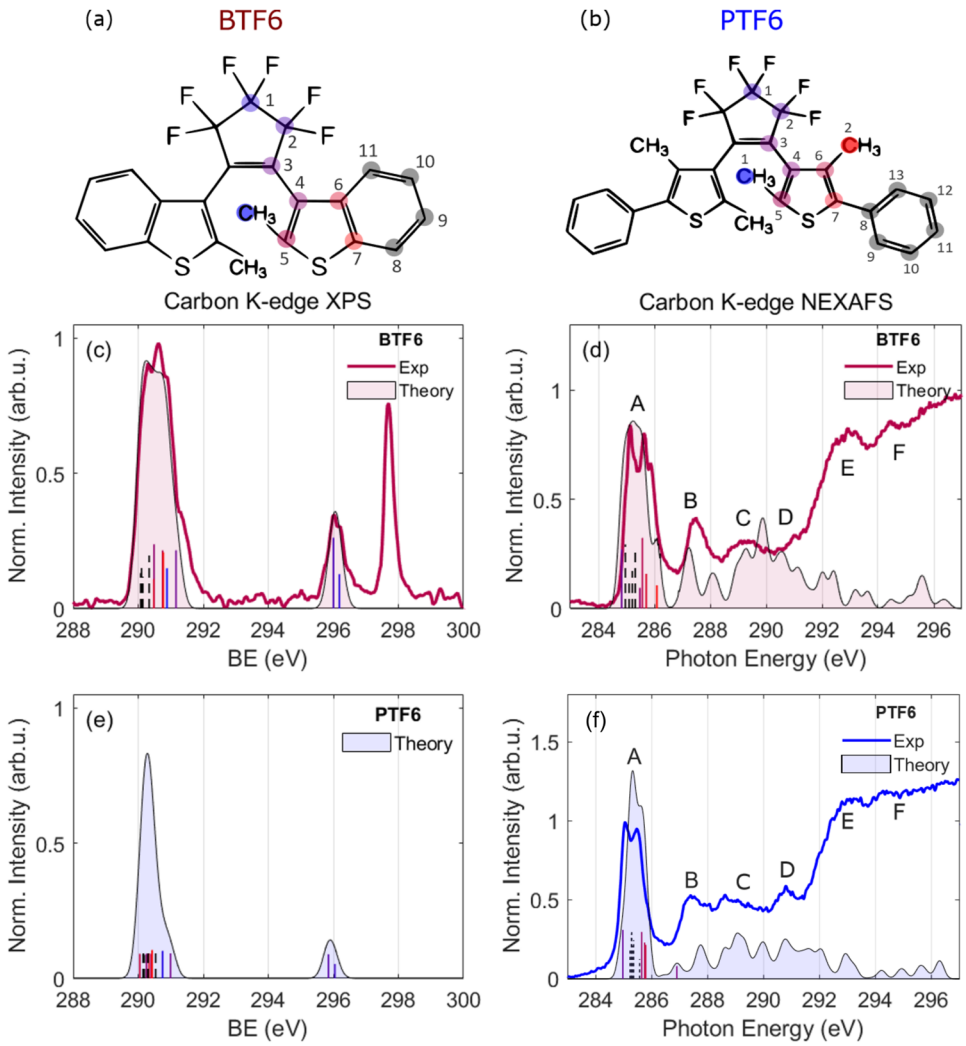

FIG. 4. Experimental data (solid line) and calculated [OR(ap) conformer, shaded area] carbon K-edge XPS and NEXAFS spectra of [(c) and (d)] BTF6 and [(e) and (f)] PTF6. Panels (a) and (b) show the carbon numbering and the color coding used in calculations at the carbon K-edge in BTF6 and PTF6, respectively. The XPS simulated spectra have been shifted by 0.25 eV, matching the experimental spectrum of BTF6. No shift has been applied to the simulated NEXAFS spectra. The peak located at 297.77 eV in the XPS at the C 1s edge of BTF6 arises from the CO_2 calibrant gas. In panels (e) and (f) are reported the carbon K-edge experimental and calculated NEXAFS spectra of BTF6 and PTF6, respectively. The NEXAFS spectra are normalized with respect to the area of peak A. Contributions from different carbon sites are highlighted by colored vertical lines; for color code, see panels (a) and (b); the numerical values are reported in Table II and Fig. 5. The dashed lines represent the contributions of the carbon atoms of the benzene aromatic rings in BTF6 and PTF6.

TABLE II. Theoretically calculated carbon K-edge binding energies (BEs) for (a) BTF6 and (b) PTF6. BEs have been shifted by 0.25 eV in both cases, as shown in Fig. 4 to match the experimental data. The different signals contributing to the spectra are due to ionization from the core orbital 1s of the C_i carbon atoms in the two molecular systems, with numeration reported in the first row of Fig. 4.

a. BTF6

Transition	BE (eV)	Dyson norm
C_1	296.19	0.74
C_2	296.00	0.73
C_3	291.16	0.65
C_4	290.49	0.65
C_5	290.75	0.62
C_6	290.48	0.66
C_7	290.77	0.66
C_8	290.33	0.62
C_9	290.14	0.63
C_{10}	290.10	0.63
C_{11}	290.08	0.64
$C(H_3)$	290.89	0.74

b. PTF6

Transition	BE (eV)	Dyson norm
C_1	296.05	0.73
C_2	295.85	0.73
C_3	290.99	0.65
C_4	290.25	0.65
C_5	290.40	0.62
C_6	290.05	0.63
C_7	290.33	0.65
C_8	290.54	0.67
C_9	290.16	0.63
C_{10}	290.30	0.63
C_{11}	290.19	0.61
C_{12}	290.30	0.63
C_{13}	290.15	0.64
$C(H_3)$	290.75	0.73
$C(H_3)$	290.43	0.73

leaving only the contributions from the pair of methyl carbons in the higher energy part. In analogy to the sulfur $L_{2,3}$-edge spectrum, we rationalize the 0.3 eV redshift with the better core-hole shielding in phenylthiophene compared to benzothiophene.

NEXAFS spectra

The measured NEXAFS spectra at the carbon K-edge are shown in Figs. 4(d) and 4(f) together with the simulated spectra, which allow us to identify the nature of the contributions over an energy range of >10 eV (284–296 eV). Transition energies, oscillator strengths, and the leading character of the transitions are reported in Fig. 5. The experimental NEXAFS spectrum of BTF6 is characterized by an intense structured band extending between 284 and 286.7 eV, peaking at 285.1 eV, followed by a broad pre-edge absorption band with peaks at 287.5 and 289.4 eV. The spectrum of PTF6 has similar features; however, it also exhibits discernible differences, namely, in PTF6, the main peak appears narrower, and a further peak emerges at 290.5 eV.

In both cases, the main peak comprises transitions from the 1s orbitals of those carbon atoms involved in the π-system to the energetically lowest unoccupied molecular orbital of π^*-character. The simulation does not perfectly capture the fine structure of the main peak, in particular in PTF6, where the computed line shape appears too narrow. Hence, the spectra were normalized with respect to the area of the main peak instead of its maximum. For each core-transition, the arrival π^* orbital is subject to a strong relaxation, which leads to its localization onto the carbon sites in immediate vicinity to the core-excited carbon atoms (see Figs. S6–S9 of the supplementary material). In both systems, the most redshifted contribution peaking at ~285.0 eV is ascribed to C_3, the reason being that the central C_3=C_3 double bond fragment is to a great extent decoupled from the rest of the π-system. As a consequence, the relaxed π^* orbital remains localized on the double bond fragment. This allows us to use the density of the excited core-electron to shield the core-hole that redshifts the energy of the core-transition. Core-transitions of benzene (C_8–C_{11} in BTF6)/phenyl (C_8–C_{13} in PTF6) carbons appear compact between 285.0 and 285.5 eV and are slightly redshifted compared to core-transitions from thiophene carbons contributing to the 285.5–286.0 eV window. The spectral features at photon energies above 286 eV can be attributed to core-transitions to orbitals of Rydberg and σ^* character. Due to their vast number and small intensities, we refrain from showing and discussing the individual transitions in the computed spectra but rather focus the discussion on entire energy ranges comprising transitions of a similar type:

1. Peak B (286.0–288.0 eV): transitions (i) from aromatic carbons toward higher lying π^* orbitals (e.g., LUMO+1 and LUMO+2); (ii) from carbons C_8–C_{11} (BTF6)/C_8–C_{13} (PTF6) toward adjacent C–H σ^* orbitals [Fig. 5(c)]; and (iii) from C_4–C_7 into the virtual orbitals of 3d and 4s characters predominantly localized on the adjacent sulfur [3d shown in Fig. 5(c)]; this set of transitions exhibits a pronounced 1.2 eV shift in PTF6 so that they contribute to peak C.
2. Peak C (288.5–289.5 eV): transitions from the carbons of the methyl groups to the adjacent C–H σ^* bonds [Fig. 5(c)]; notably, the intensity of this feature is twice as high in PTF6 due to the presence of two methyl groups; the increased intensity of this contribution, together with the blueshift of the transitions from C_4–C_7 into the sulfur orbitals of 3d and 4s, is the reason for the increased relative intensity of peak C with respect to peak B in PTF6.
3. Peak D (289.5–291.5 eV): a large number of weak transitions from aromatic carbons toward (i) quasi-Rydberg orbitals [Fig. 5(c)] and (ii) C–C σ^* bonds; this feature is somewhat more intense in PTF6 owing to the more carbons in the π-system and gives rise to the distinguishable peak in this range.
4. Peak E (292.0–293.5 eV): transitions from C_1 and C_2 toward adjacent C–F σ^* bonds [Fig. 5(c)].
5. Peak F (294.0–295.5 eV): transitions from C_1 and C_2 carbons toward adjacent C–C σ^* bonds [Fig. 5(c)].

We note the close resemblance of the spectrum of BTF6 with that of bare benzothiophene in the spectral window below

a.

Peak	Site	Energy (eV)	arrival MO
A	C_3	284.83	π^* (LUMO)
	C_4	285.48	
	C_5	285.57	
	C_6	285.71	
	C_7	286.09	
	C_8-C_{11}	285.0-285.3	
B	C_3-C_{11}	286.0-288.0	π^*
	C_8-C_{11}	287.0-287.3	$\sigma^*(C_{8-11}$-H)
	C_4-C_7	287.2-287.8	3d/4s(S)
C	$C(H_3)$,$C(H_3)$	289.0-289.3	$\sigma^*(CH_2$-H)
D	C_8-C_{11}	289.5-291.5	Ry/σ^*(C-C)
E	C_1-C_2	292.0-293.5	$\sigma^*(C_{1/2}$-F)
F	C_1-C_2	294.0-295.5	$\sigma^*(C_1$-$C_2)$

b.

Peak	Site	Energy (eV)	arrival MO
A	C_3	284.97	π^* (LUMO)
	C_4	285.67	
	C_5	285.64	
	C_6	285.75	
	C_7	285.78	
	C_8-C_{13}	285.2-285.6	
B	C_3-C_{11}	286.4-288.5	π^*
	C_8-C_{11}	287.6-287.8	$\sigma^*(C_{8-11}$-H)
C	C_4-C_7	288.5-289.0	3d(S)
	$C(H_3)$,$C(H_3)$	289.0-289.3	$\sigma^*(CH_2$-H)
D	C_8-C_{11}	289.5-291.5	Ry/σ^*(C-C)
E	C_1-C_2	292.0-293.5	$\sigma^*(C_{1/2}$-F)
F	C_1-C_2	294.0-295.5	$\sigma^*(C_1$-$C_2)$

c.

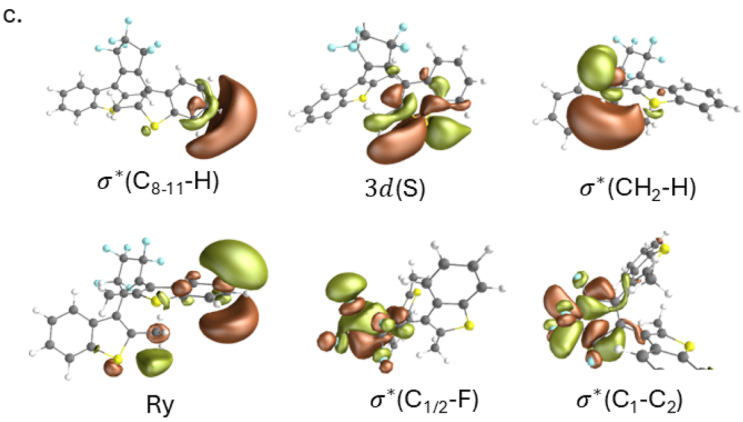

FIG. 5. Theoretically calculated core excited states at the carbon K-edge of (a) BTF6 and (b) PTF6. No shift has been applied. For each carbon contributing to the NEXAFS signal, the transition energies are reported. Only transitions from carbons having oscillator strengths larger than 10^{-4} are considered. (c) Representative arrival orbitals are shown below the table in the case of BTF6. The corresponding figure for PTF6 can be found in Fig. S12 of the supplementary material.

291 eV (see Fig. 4 of Ref. 47) and refer to the analysis performed by Toffoli *et al.*, which achieved a more complete description of the high-energy window thanks to the use of a DFT-based protocol.

PES valence-ionization spectra

Figure 6 shows the experimental and calculated valence photoelectron spectra of BTF6 and PTF6 in the BE range 7–14 eV. The simulation was carried out assuming a mixture of parallel and anti-parallel conformations of the OR form with 2:1 and 1:1 ratios for BTF6 and PTF6, respectively. This figure also reports the BE of the π orbitals of the OR(ap) conformer; the corresponding orbitals for the OR(p) conformer, as well as a full list of all 20 orbitals giving rise to the signal up to 13 eV, are reported in Figs. S12–S15 of the supplementary material.

For both systems, the spectral shape essentially mirrors the energetic order of the frontier orbitals. The signal below 11 eV is due to ionization from orbitals of π character (color sticks in Fig. 6). Instead, the signal above 11 eV is due to ionization from σ orbitals (gray sticks in Fig. 6).

Most of the orbitals show up in pairs exhibiting bonding/anti-bonding interactions between the benzothiophene or phenylthiophene units in BTF6 and PTF6, respectively. The strength of the interaction, which determines the energy splitting of each pair of signals, is susceptible to the stacking pattern in the parallel and anti-parallel conformation with chemical shifts of up to 0.25 eV. For example, in BTF6, the broad feature between BEs of 8 and 9 eV comprises contributions from two pairs of orbitals, MO1 (HOMO)/MO2, with a more pronounced contribution on the thiophene units, and MO3/MO4, exhibiting a more pronounced contribution on the benzene rings. As a consequence, in the

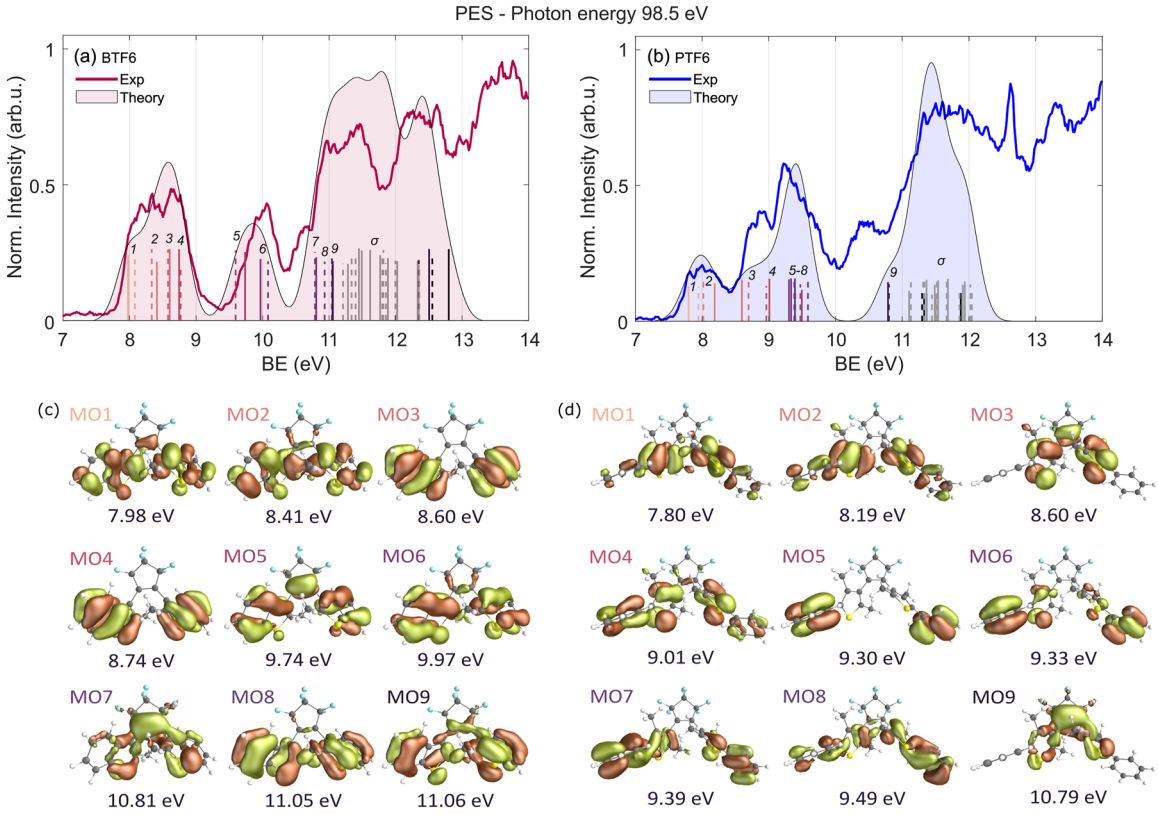

FIG. 6. Valence-ionization photoelectron spectra of (a) BTF6 and (b) PTF6, acquired with a photon energy of 98.5 eV covering a binding energy range between 7 and 14 eV. The shaded areas correspond to the calculated PES obtained assuming a mixture of OR(ap) and OR(p), with ratios 2:1 for BTF6 and 1:1 for PTF6. The simulated spectra are shifted by 0.9 eV. Vertical solid and dashed lines represent the contributions due to ionization from valence orbitals of the OR(ap) and OR(p) conformers, respectively. Colored and gray lines stand for ionization from orbitals with π and σ characters, respectively. The peak at 12.62 eV, more pronounced in the PTF6 spectrum, originates from residual water molecules present in the experimental chamber. π-type MOs of the OR(ap) conformer giving rise to the signals below 11 eV are depicted in (c) for BTF6 and (d) for PTF6. A full list of the MOs considered in the calculations, as well as the MOs of the OR(p) conformer, can be found in Figs. S12–S15 of the supplementary material.

anti-parallel conformer where the thiophene rings are spatially closer, the MO1/MO2 pair exhibits a strong 0.4 eV splitting of the associated ionization signals (peaks at 8.0 and 8.4 eV), whereas the MO3/MO4 pair exhibits a weaker splitting, which amounts to 0.15 eV (peaks at 8.5 and 8.7 eV). Instead, in the parallel conformer where the stacking involves the entire benzothiophene moieties, both pairs exhibit an intermediate splitting of 0.2 eV. MO1–4 are characterized by two nodes in the benzothiophene unit; thus, the BEs are close in value. Ionization from the next pair of orbitals MO5/MO6, which present only one node, gives rise to the separate feature at a higher BE of 10 eV, which exhibits a splitting in the OR(p) conformer twice as strong as in the OR(ap) one. The spectrum below 11 eV is completed by the ionization from a π orbital MO7 localized on the central C_3=C_3 double bond peaking at 10.5 eV, whose BE is slightly overestimated by the calculations.

In PTF6, the pronounced twisting between the thiophene and phenyl fragments localizes in both the conformers MO1/MO2 and MO3/MO4 pairs of orbitals predominantly on the thiophene ring, whereas the MO5/MO6 and MO7/MO8 pairs mostly on the phenyl. As a consequence, the splitting between signals arising from each of the first two pairs of orbital is more pronounced, especially in the anti-parallel conformer (~0.5 eV around 8 eV for MO1/MO2 and around 8.7 eV for MO3/MO4), whereas the last two pairs appear in a narrow energy range around 9.4 eV, giving rise to the sharp peak. Just as BTF6, PTF6 exhibits a peak at 10.5 eV associated with ionization from a π orbital MO9 localized on the central C3=C3 double bond, whose BE is slightly overestimated by the calculations.

Predicting transient signatures of photoinduced cyclization

The good agreement between theory and experiment regarding the spectra of the OR isomers gives us the confidence to predict the spectra of the CR isomers. This constitutes the first step in the description of photoinduced cyclization. We are aware that a complete characterization would require a time-resolved dynamical study of the evolution in the excited state and the passage through the conical intersection seam, followed by the simulation of the

transient signatures, i.e., BE and photoinduced absorption (PA) of the transient species. While this is beyond the scope of the present work, a comparison of the spectra of the OR and CR isomers offers preliminary indications about the transient signals. In Fig. 7, we report XPS at the sulfur $L_{2,3}$-edge [panel (a)] and at the carbon K-edge [panel (b)], NEXAFS at the carbon K-edge focusing only on the main peak below 286 eV [panel (c)], and PES [panel (d)] for the CR isomer of BTF6 (dashed lines) and compare them with the corresponding simulated signals of the OR (colored profile). The numerical data are provided in the supplementary material, as well as in the dedicated repository accessible via the following link: https://doi.org/10.6092/unibo/amsacta/8639. The simulation of the NEXAFS spectrum of the CR isomer at the sulfur $L_{2,3}$-edge was not attempted due to the less satisfactory agreement between theory and experiment in the OR case.

The spectral changes reflect the structural changes during the cyclization. In particular, the formation of a C5–C5 single bond enforces the planarization of the aromatic framework. The ensuing delocalization of the π-orbitals over the entire molecule has immediate consequences for core and valence spectra.

XPS at sulfur $L_{2,3}$-edge

The spectrum of the CR form is shown in Fig. 7(a). It appears redshifted by ~0.5 eV with respect to the OR form, thereby maintaining the same double peak shape. The extended π-system grants the sulfur atoms access to an extended π-electron density, which they can exploit to stabilize the core-hole more efficiently. Since the first valence excited state of BTF6 has no pronounced charge-transfer character (i.e., the electron density distribution of the ground and excited states is similar), we expect the time-resolved (TR) XPS map to show a transient signal that emerges on top of the ground state bleach of the OR form and subsequently gradually shifts toward a lower BE in the course of the cyclization.

XPS at carbon K-edge

The spectra of the OR and CR forms shown in Fig. 7(b) are very similar for the two isomers. The only difference consists in the emergence of a small peak below 292 eV due to the 0.8 eV blueshift of the signal associated with C_5 during the formation of the σ bond. The reason why the remaining carbons are not affected by the planarization of the molecule as observed in the sulfur XPS is

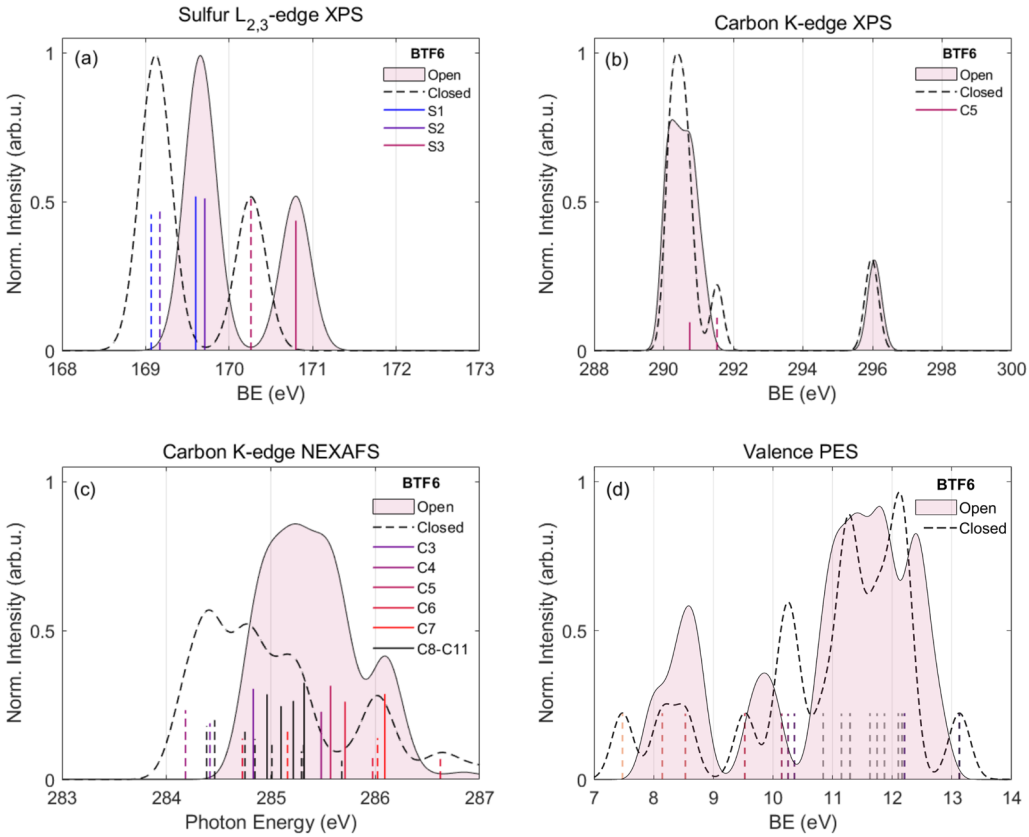

FIG. 7. Comparison between the calculated observable of the BTF6 molecule in its OR (shaded area) and CR (dashed line) conformers. In particular, (a) XPS spectra at the sulfur $L_{2,3}$-edge and (b) carbon K-edge, (c) carbon K-edge NEXAFS spectra, and (d) valence PES of BTF6 are reported, along with the significant contributions to them. All OR spectra have been computed for the anti-parallel conformer, except for the PES, which was computed for an anti-parallel:parallel ratio of 2:1.

that carbons are less electronegative compared to sulfur and as such withdraw electron density only from nearby sites to shield their core-hole. Therefore, they cannot profit from the extended form of the π-system in the CR isomer. We anticipate that the predicted additional peak at a higher BE would manifest rather as a shoulder to the main peak. Its formation might be rather cumbersome as the pair of C_5 atoms responsible for its rise represents only 10% of the total intensity in the considered window.

NEXAFS at carbon K-edge

NEXAFS spectra mirror the structure of the frontier *virtual* orbitals. In the case of the CR form of BTF6, the extension of the π-system over the entire molecule causes the energetic stabilization of those orbitals. This is reflected in a redshift of about 0.5 eV accompanied by a decrease in intensity in the main peak of the CR form, a consequence of the decreased overlap between the core orbitals and the delocalized π^* orbitals. It deserves mentioning that the contribution from C_5 is absent in the CR isomer, since it is no longer part of the conjugated system (its intensity is strongly quenched).

In the TR-NEXAFS, one generally expects to see PA contributions emerging after photo-excitation due to core-to-LUMO and core-to-HOMO transitions since both have one free vacancy in the excited state. Whereas the core-to-LUMO PA approximately falls on top of the bleach (285–286 eV), the core-to-HOMO PA feature is expected to show up strongly redshifted. The shift can be roughly estimated as the energy difference between the ground and excited states. The spectrum of the OR form of BTF6 shows an onset at about 3.5 eV (attributed to the HOMO → LUMO transition); accordingly, one could expect a transient PA around 282–283 eV and thus in an energy window free of any background from GS signals. During the motion of the system toward the conical intersection seam, these two PA features are expected to shift toward each other and progressively merge as the HOMO and LUMO become degenerate. Upon crossing the seam, the PA features should split again and converge to the signatures of the OR and CR isomers shown in Fig. 7(c).

PES

The photoemission spectra mirror the structure of the frontier *occupied* orbitals. In the case of the CR form of BTF6, the extension of the π-system over the entire molecule causes a spread of the energies of those orbitals, with the most anti-bonding one (i.e., the HOMO) ending up at higher energies compared to its counterpart in the OR form. This spread is reflected in the PES of the CR form, which shows the first peak at 7.5 eV, i.e., 0.5 eV below the lowest peak of the OR form. Moreover, features due to the ionization of π orbitals extend up to 12 eV in the CR form (compared to 11.5 eV in the OR form).

In the TR-PES, one generally expects to see signals at a low BE (below 8 eV) due to the ionization of electrons that have been promoted to virtual orbitals by the pump pulse. We expect the OR form of BTF6 to exhibit such a feature around 4 eV, i.e., the difference between the energies of the HOMO-to-LUMO transition peaking at 3.5 eV and the lowest BE in the CR PES [Fig. 7(c)] and thus in a background-free energy window. During the motion of the system toward the conical intersection seam, this feature should gradually blueshift and, upon crossing the seam, converge to the 7.5 eV peak exhibited by the CR form.

To sum up, (i) the rise of the 169 eV peak in the XPS spectrum at the sulfur $L_{2,3}$-edge, (ii) the rise of the 284 eV peak in the NEXAFS spectrum at the carbon K-edge, and (iii) the rise of the 7.5 eV peak in the PES could all be used in a time-resolved experiment to clock excited state lifetime and the time scale of the BTF6 cyclization.

CONCLUSION AND OUTLOOK

In this joint experimental and theoretical work, two representatives of the family of dithienylethenes, BTF6 and PTF6, were investigated in the gas phase by means of VUV and x-ray spectroscopies. Below, we summarize the main findings.

The sulfur atoms act largely as spectators in the electrocyclic reaction, making them less sensitive to the changes in the electronic structure. Nonetheless, the vicinity to the electrocyclic center paired with a limited number of heteroatoms gives rise to clearly discernible and easily interpretable chemical shifts. In particular, XPS at the sulfur $L_{2,3}$-edge reveals a common double peak structure, which exhibits a weak 0.2 eV redshift when replacing the benzothiophene (BTF6) with a phenylthiophene (PTF6), which can be attributed to the more extended π-system in PTF6. The redshift increases to 0.5 eV in the course of electrocyclization. The NEXAFS spectrum at the sulfur $L_{2,3}$-edge exhibits a line shape common to other thiophene-containing systems:[47] a three-peak structure with a more intense (and usually broader) middle peak, due to core excitations to a pair of virtual orbitals with 3d/4s character; its fine structure is weakly sensitive to the composition of the π-system.

The carbon atoms are more sensitive to the functionalization patterns and to the electrocyclic rearrangement. An example of the former is the nearly 5 eV blueshift of the BE for carbons bonded to fluorine in the XPS spectrum. Examples for the latter are the terminal carbon atoms in the HT unit, which show a 0.5 eV blueshift in the XPS spectrum and depletion of the NEXAFS signal upon σ-bond formation. It should be noted, however, that the spectra at the carbon K-edge are generally congested due to contributions from a large number of chemically distinct carbon sites, which complicate the analysis and often mask the signatures of the relevant atomic sites.

Finally, PES exhibits the highest degree of sensitivity to functionalization and stacking patterns and to the extension of the π-system as it probes the valence orbitals directly affected by chemical and structural changes, opposite to core-spectroscopies, which target observer orbitals. The PES line shape mirrors the electronic structure of the frontier orbitals. Strong delocalization leads to a 0.2 eV redshift of the BEs of the lowest peak as observed for PTF6 compared to BTF6. The redshift increases to 0.5 eV in the course of electrocyclization.

This study demonstrates that all the above-mentioned methods (XPS, NEXAFS, and PES) respond, albeit to a different extent, to the structural changes accompanying photoinduced cyclization. Notably, PES stands out thanks to its sensitivity to parallel and antiparallel OR conformers, which remain indistinguishable with other techniques. As such, we hope that the present work will stimulate future time-resolved investigations on DTEs in the gas phase, to be performed at XFELs and/or in HHG laboratories.

SUPPLEMENTARY MATERIAL

See the supplementary material for the mass spectrum of BTF6, the sulfur $L_{2,3}$-edge XPS spectrum of TF6, valence molecular orbitals involved in the transitions contributing to the NEXAFS and PES spectra, as well as the electronic structure of the valence-ionized, core-excited, and core-ionized levels of the closed form of BTF6.

ACKNOWLEDGMENTS

This project has received funding from the European Research Council (ERC) under the European Union's Horizon 2020 research and innovation program (Grant Agreement No. 951224, TOMATTO). M.P. and M.R. acknowledge funding from Ministero Università e Ricerca PRIN under Grant Agreement No. 2022WZ8LME. R.B.-V. and A.N. acknowledge funding from Ministero Università e Ricerca PRIN under Grant Agreement No. 202239HFZN. S.S. acknowledges funding from Fondazione Cariplo (Grant No. NR 2024-0566, ATOMS).

AUTHOR DECLARATIONS

Conflict of Interest

The authors have no conflicts to disclose.

Author Contributions

All the authors equally contributed to the review and editing of the final manuscript and the validation of the research outputs.

M. Pini: Data curation (lead); Formal analysis (equal); Investigation (equal); Methodology (equal); Visualization (lead); Writing – original draft (equal). **S. Severino**: Data curation (equal); Formal analysis (equal); Investigation (lead); Methodology (equal); Visualization (equal); Writing – original draft (equal). **L. Mai**: Investigation (equal); Methodology (equal); Writing – review & editing (equal). **L. Colaizzi**: Investigation (equal); Methodology (equal); Writing – review & editing (equal). **M. Alagia**: Data curation (supporting); Investigation (equal); Writing – review & editing (equal). **O. Plekan**: Data curation (supporting); Investigation (equal); Writing – review & editing (equal). **R. Richter**: Investigation (equal); Writing – review & editing (equal). **E. Arfaoui**: Formal analysis (supporting); Writing – review & editing (equal). **F. Montorsi**: Formal analysis (supporting); Writing – review & editing (equal). **F. Segatta**: Formal analysis (supporting); Writing – review & editing (equal). **M. Garavelli**: Funding acquisition (supporting); Writing – review & editing (equal). **S. Aloïse**: Conceptualization (supporting); Investigation (supporting); Writing – review & editing (equal). **L. Poisson**: Conceptualization (supporting); Investigation (supporting); Writing – review & editing (equal). **R. Borrego-Varillas**: Conceptualization (supporting); Writing – review & editing (equal). **M. Lucchini**: Conceptualization (supporting); Writing – review & editing (equal). **M. Coreno**: Data curation (supporting); Investigation (equal); Writing – review & editing (equal). **M. Nisoli**: Conceptualization (supporting); Funding acquisition (lead); Writing – review & editing (equal). **M. Reduzzi**: Conceptualization (equal); Formal analysis (equal); Funding acquisition (equal); Investigation (equal); Methodology (equal); Project administration (equal); Supervision (equal); Visualization (equal); Writing – original draft (equal). **A. Nenov**: Conceptualization (equal); Formal analysis (equal); Investigation (equal); Methodology (equal); Supervision (equal); Visualization (equal); Writing – original draft (equal).

DATA AVAILABILITY

The data that support the findings of this study are openly available in AMS Acta at https://doi.org/10.6092/unibo/amsacta/8639.

REFERENCES

[1] M. Irie and M. Morimoto, "Molecular photoswitches: Fundamentals and applications of diarylethenes," in *Photochemistry* (The Royal Society of Chemistry, 2019), Vol. 47, p. 457.
[2] M. Irie, T. Fukaminato, K. Matsuda, and S. Kobatake, "Photochromism of diarylethene molecules and crystals: Memories, switches, and actuators," Chem. Rev. **114**(24), 12174–12277 (2014).
[3] C. Jia, A. Migliore, N. Xin, S. Huang, J. Wang, Q. Yang, S. Wang, H. Chen, D. Wang, B. Feng, Z. Liu, G. Zhang, D.-H. Qu, H. Tian, M. A. Ratner, H. Q. Xu, A. Nitzan, and X. Guo, "Covalently bonded single-molecule junctions with stable and reversible photoswitched conductivity," Science **352**(6292), 1443–1445 (2016).
[4] H. Cahová and A. Jäschke, "Nucleoside-based diarylethene photoswitches and their facile incorporation into photoswitchable DNA," Angew. Chem., Int. Ed. **52**(11), 3186–3190 (2013).
[5] Y. Zou, T. Yi, S. Xiao, F. Li, C. Li, X. Gao, J. Wu, M. Yu, and C. Huang, "Amphiphilic diarylethene as a photoswitchable probe for imaging living cells," J. Am. Chem. Soc. **130**(47), 15750–15751 (2008).
[6] Y. Ishibashi, M. Fujiwara, T. Umesato, H. Saito, S. Kobatake, M. Irie, and H. Miyasaka, "Cyclization reaction dynamics of a photochromic diarylethene derivative as revealed by femtosecond to microsecond time-resolved spectroscopy," J. Phys. Chem. C **115**(10), 4265–4272 (2011).
[7] A. Jarota, E. Pastorczak, W. Tawfik, B. Xue, R. Kania, H. Abramczyk, and T. Kobayashi, "Exploring the ultrafast dynamics of a diarylethene derivative using sub-10 fs laser pulses," Phys. Chem. Chem. Phys. **21**, 192–204 (2019).
[8] S. M. Mendoza, M. Lubomska, M. Walko, B. L. Feringa, and P. Rudolf, "Characterization by X-ray photoemission spectroscopy of the open and closed forms of a dithienylethene switch in thin films," J. Phys. Chem. C **111**(44), 16533–16537 (2007).
[9] H. Jean-Ruel, M. Gao, M. A. Kochman, C. Lu, L. C. Liu, R. R. Cooney, C. A. Morrison, and R. J. D. Miller, "Ring-closing reaction in diarylethene captured by femtosecond electron crystallography," J. Phys. Chem. B **117**(49), 15894–15902 (2013).
[10] M. Boggio-Pasqua, M. Ravaglia, M. J. Bearpark, M. Garavelli, and M. A. Robb, "Can diarylethene photochromism be explained by a reaction path alone? A CASSCF study with model MMVB dynamics," J. Phys. Chem. A **107**(50), 11139–11152 (2003).
[11] Y. Asano, A. Murakami, T. Kobayashi, A. Goldberg, D. Guillaumont, S. Yabushita, M. Irie, and S. Nakamura, "Theoretical study on the photochromic cycloreversion reactions of dithienylethenes; on the role of the conical intersections," J. Am. Chem. Soc. **126**(38), 12112–12120 (2004).
[12] A. Perrier, S. Aloise, M. Olivucci, and D. Jacquemin, "Inverse versus normal dithienylethenes: Computational investigation of the photocyclization reaction," J. Phys. Chem. Lett. **4**(13), 2190–2196 (2013).
[13] I. Hamdi, G. Buntinx, A. Perrier, O. Devos, N. Jaïdane, S. Delbaere, A. K. Tiwari, J. Dubois, M. Takeshita, Y. Wada, and S. Aloïse, "New insights into the photoswitching mechanisms of normal dithienylethenes," Phys. Chem. Chem. Phys. **18**, 28091–28100 (2016).
[14] I. Hamdi, G. Buntinx, O. Poizat, S. Delbaere, A. Perrier, R. Yamashita, K.-i. Muraoka, M. Takeshita, and S. Aloïse, "Unraveling ultrafast dynamics of the photoswitchable bridged dithienylethenes under structural constraints," Phys. Chem. Chem. Phys. **21**, 6407–6414 (2019).
[15] T. Yanai, M. Saitow, X.-G. Xiong, J. Chalupský, Y. Kurashige, S. Guo, and S. Sharma, "Multistate complete-active-space second-order perturbation theory

based on density matrix renormalization group reference states," J. Chem. Theory Comput. **13**(10), 4829–4840 (2017).
[16]A. Jarota, E. Pastorczak, and H. Abramczyk, "A deeper look into the photocycloreversion of a yellow diarylethene photoswitch: Why is it so fast?," Phys. Chem. Chem. Phys. **22**, 5408–5412 (2020).
[17]J. Jankowska, M. Martyka, and M. Michalski, "Photo-cycloreversion mechanism in diarylethenes revisited: A multireference quantum-chemical study at the ODM2/MRCI level," J. Chem. Phys. **154**(20), 204305 (2021).
[18]M. Martyka and J. Jankowska, "Nonadiabatic molecular dynamics study of a complete photoswitching cycle for a full-size diarylethene system," J. Photochem. Photobiol., A **438**, 114513 (2023).
[19]M. Martyka and J. Jankowska, "New insights into the photocyclization reaction of a popular diarylethene switch: A nonadiabatic molecular dynamics study," Phys. Chem. Chem. Phys. **26**, 13383–13394 (2024).
[20]C. Climent, Z. Xu, M. O. Wolf, and D. Casanova, "Predictive guidelines for electrocyclization of dithienylethenes," J. Phys. Chem. Lett. **15**(31), 8042–8048 (2024).
[21]A. Jarota and E. Pastorczak, "Tale of three dithienylethenes: Following the photocycloreversion with ultrafast spectroscopy and quantum dynamics simulations," J. Phys. Chem. B **129**(5), 1605–1613 (2025).
[22]A. Lietard, G. Piani, R. Pollet, B. Soep, J.-M. Mestdagh, and L. Poisson, "Excited state dynamics of normal dithienylethene molecules either isolated or deposited on an argon cluster," Phys. Chem. Chem. Phys. **24**, 10588–10598 (2022).
[23]M. G. Delcey, L. K. Sørensen, M. Vacher, R. C. Couto, and M. Lundberg, "Efficient calculations of a large number of highly excited states for multiconfigurational wavefunctions," J. Comput. Chem. **40**(19), 1789–1799 (2019).
[24]A. Nenov, F. Segatta, A. Bruner, S. Mukamel, and M. Garavelli, "X-ray linear and non-linear spectroscopy of the ESCA molecule," J. Chem. Phys. **151**(11), 114110 (2019).
[25]F. Montorsi, F. Segatta, A. Nenov, S. Mukamel, and M. Garavelli, "Soft X-ray spectroscopy simulations with multiconfigurational wave function theory: Spectrum completeness, sub-eV accuracy, and quantitative reproduction of line shapes," J. Chem. Theory Comput. **18**(2), 1003–1016 (2022).
[26]L. Carlini, F. Montorsi, Y. Wu, P. Bolognesi, R. Borrego-Varillas, A. R. Casavola, M. C. Castrovilli, J. Chiarinelli, D. Mocci, F. Vismarra, M. Lucchini, M. Nisoli, S. Mukamel, M. Garavelli, R. Richter, A. Nenov, and L. Avaldi, "Electron and ion spectroscopy of azobenzene in the valence and core shells," J. Chem. Phys. **158**(5), 054201 (2023).
[27]L. Oberti, L. Avaldi, P. Bolognesi, M. Bonanomi, R. Borrego-Varillas, C. Callegari, L. Carlini, J. Chiarinelli, E. Ciekalski, M. Coreno, M. Devetta, M. Di Fraia, M. Garavelli, M. Goffe, C. Grazioli, F. Montorsi, K. C. Prince, R. Richter, F. Segatta, S. Waldmannstetter, G. Cerullo, H. Dube, O. Plekan, D. Faccialà, C. Vozzi, and A. Nenov, "Characterization of the hemithioindigo photoswitch and its derivatives with X-ray photoabsorption and photoemission spectroscopies," J. Chem. Phys. **162**(24), 244202 (2025).
[28]R. R. Blyth, R. Delaunay, M. Zitnik, J. Krempasky, R. Krempaska, J. Slezak, K. C. Prince, R. Richter, M. Vondracek, R. Camilloni, L. Avaldi, M. Coreno, G. Stefani, C. Furlani, M. De Simone, S. Stranges, and M. Y. Adam, "The high resolution gas phase photoemission beamline, ELETTRA," J. Electron Spectrosc. Relat. Phenom. **101–103**, 959–964 (1999).
[29]M. Alagia, L. Avaldi, M. Coreno, R. Camilloni, C. Furlani, K. C. Prince, R. Richter, M. de Simone, G. Stefani, and S. Stranges, "The gas phase photoemission beamline at ELETTRA," Synchrotron Radiat. News **16**(2), 19–27 (2003).
[30]L. Pettersson, J. Nordgren, L. Selander, C. Nordling, K. Siegbahn, and H. Ågren, "Core-electron binding energies in the soft X-ray range obtained in X-ray emission," J. Electron Spectrosc. Relat. Phenom. **27**(1), 29–37 (1982).
[31]V. Myrseth, J. D. Bozek, E. Kukk, L. J. Sæ thre, and T. D. Thomas, "Adiabatic and vertical carbon 1s ionization energies in representative small molecules," J. Electron Spectrosc. Relat. Phenom. **122**(1), 57–63 (2002).
[32]E. Hudson, D. A. Shirley, M. Domke, G. Remmers, A. Puschmann, T. Mandel, C. Xue, and G. Kaindl, "High-resolution measurements of near-edge resonances in the core-level photoionization spectra of SF_6," Phys. Rev. A **47**, 361–373 (1993).
[33]M. Tronc, G. C. King, and F. H. Read, "Carbon K-shell excitation in small molecules by high-resolution electron impact," J. Phys. B: At. Mol. Phys. **12**(1), 137 (1979).
[34]D. W. Turner, C. Baker, A. D. Baker, and C. R. Brundle, *Molecular Photoelectron Spectroscopy* (Wiley-Interscience, London, 1970).
[35]S. Severino, F. Aleotti, L. Mai, A. Crego, F. Medeghini, F. Frassetto, L. Poletto, M. Lucchini, F. Segatta, M. Reduzzi, M. Nisoli, A. Nenov, and R. Borrego-Varillas, "Mapping excited-state decay mechanisms in acetylacetone by sub-20 fs time-resolved photoelectron spectroscopy," J. Am. Chem. Soc. **147**(34), 30785–30793 (2025).
[36]P. Å. Malmqvist, A. Rendell, and B. O. Roos, "The restricted active space self-consistent-field method, implemented with a split graph unitary group approach," J. Phys. Chem. **94**(14), 5477–5482 (1990).
[37]P. Å. Malmqvist, K. Pierloot, A. R. M. Shahi, C. J. Cramer, and L. Gagliardi, "The restricted active space followed by second-order perturbation theory method: Theory and application to the study of CuO_2 and Cu_2O_2 systems," J. Chem. Phys. **128**(20), 204109 (2008).
[38]B. N. C. Tenorio, A. Ponzi, S. Coriani, and P. Decleva, "Photoionization observables from multi-reference Dyson orbitals coupled to B-spline DFT and TD-DFT continuum," Molecules **27**(4), 1203 (2022).
[39]P.-Å. Malmqvist and B. O. Roos, "The CASSCF state interaction method," Chem. Phys. Lett. **155**(2), 189–194 (1989).
[40]G. Li Manni, I. F. Galván, A. Alavi, F. Aleotti, F. Aquilante, J. Autschbach, D. Avagliano, A. Baiardi, J. J. Bao, S. Battaglia, L. Birnoschi, A. Blanco-González, S. I. Bokarev, R. Broer, R. Cacciari, P. B. Calio, R. K. Carlson, R. Carvalho Couto, L. Cerdán, L. F. Chibotaru, N. F. Chilton, J. R. Church, I. Conti, S. Coriani, J. Cuéllar-Zuquin, R. E. Daoud, N. Dattani, P. Decleva, C. de Graaf, M. G. Delcey, L. De Vico, W. Dobrautz, S. S. Dong, R. Feng, N. Ferré, M. Filatov (Gulak), L. Gagliardi, M. Garavelli, L. González, Y. Guan, M. Guo, M. R. Hennefarth, M. R. Hermes, C. E. Hoyer, M. Huix-Rotllant, V. K. Jaiswal, A. Kaiser, D. S. Kaliakin, M. Khamesian, D. S. King, V. Kochetov, M. Krośnicki, A. A. Kumaar, E. D. Larsson, S. Lehtola, M.-B. Lepetit, H. Lischka, P. López Ríos, M. Lundberg, D. Ma, S. Mai, P. Marquetand, I. C. D. Merritt, F. Montorsi, M. Mörchen, A. Nenov, V. H. A. Nguyen, Y. Nishimoto, M. S. Oakley, M. Olivucci, M. Oppel, D. Padula, R. Pandharkar, Q. M. Phung, F. Plasser, G. Raggi, E. Rebolini, M. Reiher, I. Rivalta, D. Roca-Sanjuán, T. Romig, A. A. Safari, A. Sánchez-Mansilla, A. M. Sand, I. Schapiro, T. R. Scott, J. Segarra-Martí, F. Segatta, D.-C. Sergentu, P. Sharma, R. Shepard, Y. Shu, J. K. Staab, T. P. Straatsma, L. K. Sřrensen, B. N. C. Tenorio, D. G. Truhlar, L. Ungur, M. Vacher, V. Veryazov, T. A. Voß, O. Weser, D. Wu, X. Yang, D. Yarkony, C. Zhou, J. P. Zobel, and R. Lindh, "The OpenMolcas *web*: A community-driven approach to advancing computational chemistry," J. Chem. Theory Comput. **19**(20), 6933–6991 (2023).
[41]M. J. Frisch, G. W. Trucks, H. B. Schlegel, G. E. Scuseria, M. A. Robb, J. R. Cheeseman, G. Scalmani, V. Barone, G. A. Petersson, H. Nakatsuji, X. Li, M. Caricato, A. V. Marenich, J. Bloino, B. G. Janesko, R. Gomperts, B. Mennucci, H. P. Hratchian, J. V. Ortiz, A. F. Izmaylov, J. L. Sonnenberg, D. Williams-Young, F. Ding, F. Lipparini, F. Egidi, J. Goings, B. Peng, A. Petrone, T. Henderson, D. Ranasinghe, V. G. Zakrzewski, J. Gao, N. Rega, G. Zheng, W. Liang, M. Hada, M. Ehara, K. Toyota, R. Fukuda, J. Hasegawa, M. Ishida, T. Nakajima, Y. Honda, O. Kitao, H. Nakai, T. Vreven, K. Throssell, J. A. Montgomery, Jr., J. E. Peralta, F. Ogliaro, M. J. Bearpark, J. J. Heyd, E. N. Brothers, K. N. Kudin, V. N. Staroverov, T. A. Keith, R. Kobayashi, J. Normand, K. Raghavachari, A. P. Rendell, J. C. Burant, S. S. Iyengar, J. Tomasi, M. Cossi, J. M. Millam, M. Klene, C. Adamo, R. Cammi, J. W. Ochterski, R. L. Martin, K. Morokuma, O. Farkas, J. B. Foresman, and D. J. Fox, *Gaussian 16, Revision A.03*, Gaussian, Inc., Wallingford, CT, 2016.
[42]J. P. Zobel, P.-O. Widmark, and V. Veryazov, "The ANO-R basis set," J. Chem. Theory Comput. **16**(1), 278–294 (2020).
[43]D. Peng and M. Reiher, "Exact decoupling of the relativistic Fock operator," Theor. Chem. Acc. **131**(1), 1081 (2012).
[44]T. B. Pedersen, S. Lehtola, I. Fdez Galván, and R. Lindh, "The versatility of the Cholesky decomposition in electronic structure theory," Wiley Interdiscip. Rev.: Comput. Mol. Sci. **14**(1), e1692 (2024).
[45]S. Kobatake, T. Yamada, K. Uchida, N. Kato, and M. Irie, "Photochromism of 1,2-bis(2,5-dimethyl-3-thienyl)perfluorocyclopentene in a single crystalline phase," J. Am. Chem. Soc. **121**(11), 2380–2386 (1999).
[46]M. Irie, K. Uchida, T. Eriguchi, and H. Tsuzuki, "Photochromism of single-crystalline diarylethenes," Chem. Lett. **24**(10), 899–900 (1995).

[47]D. Toffoli, A. Guarnaccio, C. Grazioli, T. Zhang, F. Johansson, M. de Simone, M. Coreno, A. Santagata, M. D'Auria, C. Puglia, E. Bernes, M. Stener, and G. Fronzoni, "Electronic structure characterization of a thiophene benzo-annulated series of common building blocks for donor and acceptor compounds studied by gas phase photoelectron and photoabsorption synchrotron spectroscopies," J. Phys. Chem. A **122**(44), 8745–8761 (2018).
[48]In the absence of spin–orbit coupling, all three 2*p* orbitals have a nearly degenerate BE.
[49]O. Baseggio, D. Toffoli, M. Stener, G. Fronzoni, M. de Simone, C. Grazioli, M. Coreno, A. Guarnaccio, A. Santagata, and M. D'Auria, "S_{2p} core level spectroscopy of short chain oligothiophenes," J. Chem. Phys. **147**(24), 244301 (2017).
[50]O. Plekan, A. Ponzi, C. Grazioli, M. Coreno, M. de Simone, F. Morini, E. Bernes, G. Fronzoni, and D. Toffoli, "Electronic structure of 2(5H)-thiophenone studied by UPS and soft X-ray spectroscopy," J. Phys. B: At., Mol. Opt. Phys. **58**(1), 015101 (2024).